Thin Solid Films 638 (2017) 389–395

Contents lists available at ScienceDirect

Thin Solid Films

journal homepage: www.elsevier.com/locate/tsf

Influence of oxygen concentration on the optoelectronic properties of hydrogenated polymorphous silicon thin films

J.D. Escobar-Carrasquilla [a], C. Álvarez-Macías [b,*], A. Dutt [a], E. Mon-Pérez [a], L. Huerta [a], G. Santana [a,*]

[a] Instituto de Investigaciones en Materiales, Universidad Nacional Autónoma de México, A.P. 70-360, Coyoacán C.P. 04510, D.F., Mexico
[b] Instituto Tecnológico de la Laguna, División de Estudios de Posgrado e Investigación, Boulevard Revolución y Av. Instituto Tecnológico de la Laguna s/n, Col. Centro, Apartado postal 681, C.P. 27000 Torreón, Coahuila, Mexico

ARTICLE INFO

Article history:
Received 9 December 2016
Received in revised form 2 August 2017
Accepted 2 August 2017
Available online 4 August 2017

Keywords:
Plasma-enhanced chemical vapor deposition
Hydrogenated polymorphous silicon
Oxygen concentration
X-ray photoelectron spectroscopy
Optoelectronic properties
Conductivity

ABSTRACT

Hydrogenated polymorphous silicon (pm-Si:H) is a suitable candidate for application in silicon-based thin film solar cells because it exhibits improved electronic transport properties and stability with respect to conventional hydrogenated amorphous silicon (a-Si:H). The use of chlorinated precursors to grow pm-Si:H thin films in a plasma enhanced chemical vapor deposition systems increases photoconductivity and photo-stability, which is one of the most desired aspects for modern solar cell applications. However, the effects of chlorine and hydrogen chemistry should be more extensively studied because it may lead to the generation of a secondary SiO_x phase, after exposure to the ambiance and/or during the growth processes. In the present work, X-Ray photoelectron spectroscopy results showed the depth profile of oxygen in the polymorphous silicon thin film. Finally, we have analyzed the effect of different concentrations and profile of oxygen on the electronic transport properties by means of dark and photoconductivity analysis. Sample with high crystalline fraction and oxygen concentration showed an increase in photo-stability and conductivity due to the passivation of free terminal bonds with oxygen. Understanding chemical and structural properties of pm-Si: H thin films based on chlorine, with additional oxygen incorporation to the films, is a key towards optimizing their electrical and optical properties for the practical implementation of solar cells.

© 2017 Elsevier B.V. All rights reserved.

1. Introduction

Hydrogenated polymorphous silicon (pm-Si:H) is one of the promising materials for thin-film solar cells due to its lower density of localized gap states and better transport properties [1]. Furthermore, it exhibits improved stability with respect to hydrogenated amorphous silicon (a-Si:H) after light-soaking experiments [2,3]. Normally, pm-Si:H films have been deposited using highly diluted silane (hydrogen mixtures) in a plasma enhanced chemical vapor deposition (PECVD) process. The use of high hydrogen dilutions is necessary to obtain thin films with sufficient crystalline fraction and lower density of localized gap states, however, at the same time, it also invokes the excessive incorporation of weak Si—H bonds into the a-Si thin-film, which is unsuitable for photovoltaic applications [4–6]. In the earlier reports, the use of silicon chlorinated precursors, as SiH_2Cl_2 and $SiCl_4$, has been used aiming at the improvement of material properties [5–9]. The use of chlorine in PECVD processes has shown many advantages such as i) increasing crystallization processes, in contrast with SiH_4, ii) post thermal annealing is not necessary for the formation of nanoparticles and iii) minor incorporation of weak Si—H bonds, which could favor the stability of thin films [10,11]. Until date, there exist many reports about the different nucleation and growth mechanism for the crystallization process of silicon thin films [12,13]. However, the chlorine-terminated surface with a strong electronegative state can preferentially react with residual oxygen and water vapor (hydrolysis reaction) forming SiO and SiOH complexes with a higher degree of disorder in the network. This process could occur due to the preferential abstraction of H and Cl from the growing surface because the coexistence of H and Cl is chemically and thermally unstable [14]. Even, silicon oxide materials are being investigated for their use in thin film silicon solar cells because they exhibit low absorption and low refractive index, owing to the incorporated oxygen [15–19]. Furthermore, it has been shown that a small amount of oxygen in a μc-network, could result in a wide band gap material, with a reasonable conductivity and could also result in the decay of electrical properties of the films [16]. As well, it has been reported that the electronegativity of the oxygen atoms and its incorporation into an a-Si:H network could cause the formation of dangling bonds [17]. As mentioned above this could cause the formation of a more disordered structure, resulting in the decrement of electrical properties of the thin films. However, in the case of pm-Si:H films there are no

* Corresponding authors.
E-mail addresses: alvarez.krlos@gmail.com (C. Álvarez-Macías), gsantana@iim.unam.mx (G. Santana).

http://dx.doi.org/10.1016/j.tsf.2017.08.004
0040-6090/© 2017 Elsevier B.V. All rights reserved.

reports, until now, which demonstrates the influence of oxygen corporation in the matrix.

In this work, we examined the role of oxygen concentration on the structural parameters and its relative effect on the optoelectronic properties of pm-Si thin films over time, deposited by PECVD using dichlorosilane. We analyze the effects of light–soaking annealing on the conductivity measurements (dark and photo, respectively), oxidation level, crystalline fractions and chemical composition of the pm-Si:H thin films for various optoelectronic applications.

2. Experimental

pm-Si:H thin films were grown in a conventional PECVD system with parallel plates of 150 cm^2 and 1.5 cm apart, activated by an RF signal of 13.56 MHz, using a mixture of SiH_2Cl_2 (99.99%) and H_2 (99.999%) [7,20]. Depositions were performed at two different pressures of 33.33 and 66.66 Pa and at H_2 flow rates of 25, 50, 75 and 100 sccm, keeping the other deposition parameters constant. Hydrogen dilution ratio, R_H was maintained during the depositions as ($R_H = H_2/(SiH_2Cl_2 + H_2)$). Nano-structural characterization of the samples was performed using Raman spectroscopy with a Horiba Jobin-Yvon triple monochromator; further details can be reviewed at [7,10]. X-ray photoelectron spectroscopy (XPS) analyses were performed in an ultra-high vacuum (UHV) system VG-Scientific Microtech Multilab ESCA2000, with a Mg K_ X-ray source ($h\nu = 1486.6$ eV), and a CLAM4 MCD analyzer. The surface of the samples was etched for 15 min with 3:0 kV Ar^+ at 0.04 μAmm^{-2}. The XPS spectra were obtained at 55 degrees to the normal surface in the constant pass energy mode (CAE), E0 = 50 and 20 eV for surface and high-resolution narrow scan, respectively. The peak positions were referenced to the background silver $3d_{5/2}$ photopeak at 368:20 eV, having a full width half maximum (FWHM) of 1:00 eV, and C 1s hydrocarbon groups at 285:00 eV central peak core level position. The XPS spectra were fitted using the SDP v 4:1 program.

Fourier transform infrared (FTIR) spectra of the films were recorded in absorbance mode using a Nicolet-210 FTIR spectrometer in the range 400–4000 cm^{-1} on thin-film samples deposited on single side polished crystalline silicon substrates. Optical properties were deduced from the absorption spectrum by a JASCO V630 UV-VIS spectrometer and using the Tauc Model [21], and the films thicknesses were obtained by typical profilometry and were cross-checked by cross section micrographs from scanning electron microscopy (SEM).

The light soaking treatment was realized in homemade equipment based on a Faraday shield, which isolates electrical and optical noise. The dark conductivity, σ_d, and photoconductivity, σ_{ph}, were obtained by two-point probes method. Fixed voltage was applied, and further, dark and photocurrents were calculated respectively. Calculations were made using the following formula [19]:

$$\sigma = \frac{I \cdot W}{L \cdot d \cdot V} \tag{1}$$

Where I is the loop current, W is the electrodes width, L is the length of the electrode, d is the film thickness, and V is the bias voltage. The factor photoconductivity is very important characteristic for the quality check of optoelectronic devices as it is directly correlated with the parameter $\mu\tau$ (inversely proportional to the concentration of dangling bonds in the thin film).

Growth conditions of the samples, results of structural parameters (Crystalline Fraction: X_c and the average size of silicon nanoparticle: D_R) and oxygen concentration (subdivided into two different groups depending on concentration) are termed (**N** with less oxygen concentration and **O** with more oxygen concentration) are summarized in Table 1.

Table 1
Growth conditions and structural parameters of the samples of pm-Si: H thin films deposited by PECVD and are organized according to low and high oxygen concentrations.

Growth conditions				Structural parameters	
RF power density = 150 W, flows: Ar = 50 sccm and SiH_2Cl_2 = 5 sccm. $T_{substrate}$ = 200 °C. Time of growth 30 min					
Sample	Pressure [Pa]	Dilution R_H [%]	Growth rate (nm/min)	X_C [%]	D_R [nm]
Samples with oxygen concentration < 15%					
N1	66.66	90.9	8.2	65	3.1
N2	33.33	93.8	10.1	69	3.2
N3	33.33	83.3	9.1	70	2.7
N4	33.33	90.9	10.8	83	2.4
N5	66.66	83.3	7.8	92	2.8
Samples with oxygen concentration > 25%					
O1	33.33	95.2	11.8	94	4.2
O2	66.66	95.2	10.4	94	3.4
O3	66.66	93.8	9.4	95	3.3

3. Results and discussion

For the better understanding, the samples in Table 1 are separated depending on the oxidation level based on the results obtained from XPS analysis (Fig. 1). Further, depending on the oxygen concentration, samples are subdivided into two groups such as <15%, designated as N1, N2, N3, N4 and N5, and >25% labeled as O1, O2, and O3. Moreover, structural parameters illustrated in Table 1 were also obtained from deconvolution analysis of Raman spectra as demonstrated in our previous work [7]. It can be observed from Table 1 that the samples O1, O2, and O3 have the highest structural parameters which include the factors like crystalline volume fraction, X_C, and the mean grain size, D_R, which indicates the highest degree of crystallization of these thin films. Besides, we can see that these samples were grown at high hydrogen dilution, R_H, and high deposition pressure. Incrementing above mentioned conditions (deposition pressure as well as hydrogen dilution) in the growth process could cause subsequent decomposition of precursors gas more efficiently and as well could promote the effective interaction of atomic H, Si—H, and Si—Cl bonds. It could result in a higher density of nucleation sites and increased chlorine extraction from the thin film. Furthermore, it could also cause an enhancement of ion bombardment and attack on the growing surface [10]. This can be cross confirmed in the form of surface porosity of thin films which could promote the post-deposition oxidation by hydrolysis reactions in response to exposure.

3.1. XPS analysis

Fig. 1 shows the high-resolution XPS spectra (deconvolution) results. Depending on the preparation conditions, it can be observed the incorporation of terminal chlorine into *Si*-O-Cl bonds type, which could produce stoichiometric Si—O oxidation states below the growing surface of the thin film, without preforming Si—Cl bond type. In the XPS analysis, five oxidation states have been identified for silicon; these chemical states are directly related to the oxygen present in the thin film and are promoted by the presence of chlorine, corresponding oxidations states are as; Si. Si_2O, SiO, Si_2O_3 and SiO_2, respectively.

From the deconvolution of the different oxidation states, binding energy (BE) for the Si 2p core level were determined as; Si^0 BE = 99.50 eV, Si^{1+} at 100.45 eV, Si^{2+} at 101.25 eV, Si^{3+} at 101.98 eV and Si^{4+} at 103.40 eV. On the other hand, for O-1s core level corresponding oxidation states were determined as, O^{1-} BE = 531.45 eV, O^{2-} in 532.29 eV, O^{3-} in 532.33 eV and O^{4-} in 532.77 eV. Likewise, it was observed that Cl-2p is found in small proportions within the films and its main activity is to stabilize the surface of the thin film [22,23]. The most abundant chlorine content was determined in sample O3, with 5.2% in elemental proportion [24]. Quantitative analysis performed by XPS in most cases

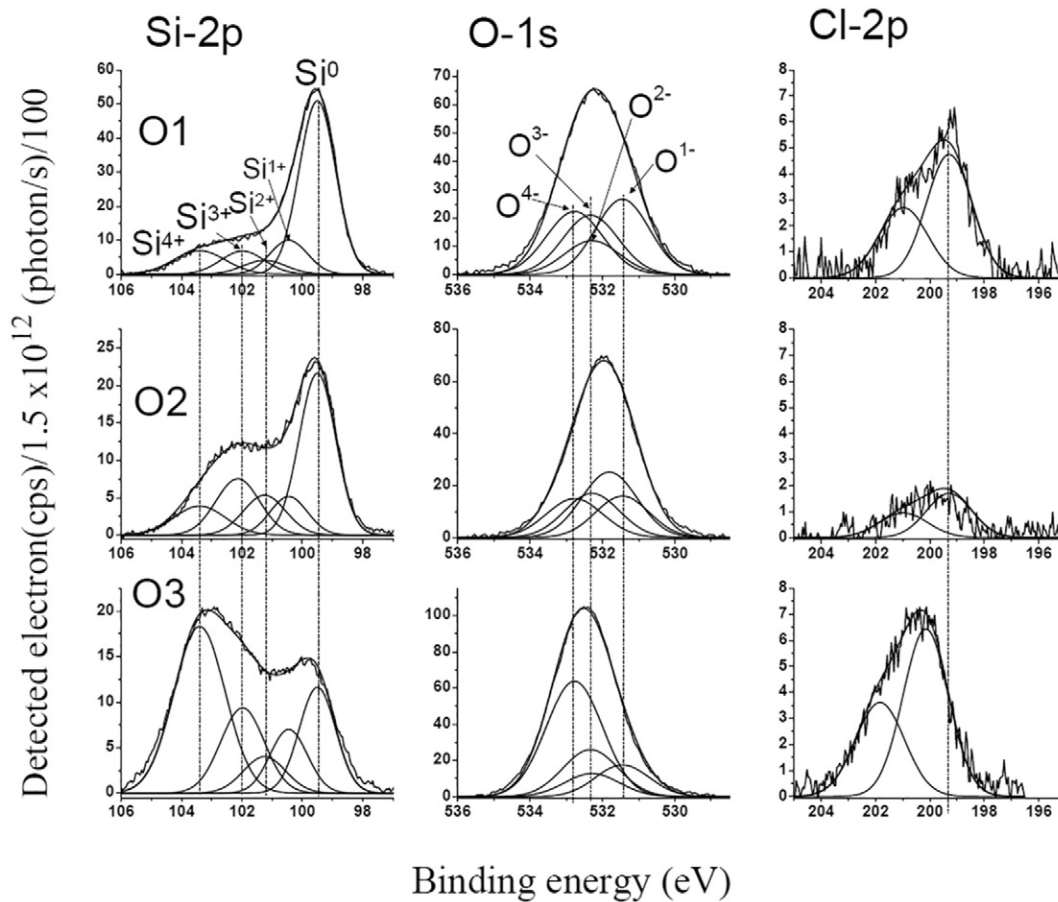

Fig. 1. Representative deconvolutions of the Si-2p, O—1S and Cl-2p peaks for samples O1, O2 and O3 deposited at different growth conditions.

use empirical calibration constants (called atomic sensitivity factors, ASF) derived from standards, measuring the peak areas of elemental core level (I) and by applying ASF, using the equation:

$$Cx = (Ix/ASFx)/\left(\sum Ii/ASFi\right)$$

where Cx is the atomic fraction of element x in a sample. The sensitivity factors can be calculated theoretically or derived empirically from the analysis of standard samples. Peak areas are defined by applying an appropriate background correction across the binding energy range of the peaks of element core level.

From the analysis illustrated in Fig. 1 of XPS, elemental concentration of different species has been reported in Table 2.

These samples were grown at a dilution $R_H = 93.8\%$ and a pressure of 66.66 Pa, presenting the slowest growth rate of the film in the order of 9.4 nm/min. This could cause the chlorine to be trapped in the structure of the sample. On the other hand, sample O2 grown at the same pressure but with a higher dilution $R_H = 95.2\%$, showed a higher growth rate (see Table 1) and lower chlorine concentration of 1.7%. Finally, sample O1 with a lower pressure than the previous ones of 33.33 Pa, but the same R_H as that of sample O2, presents the greater speed of growth with an atomic percentage of 3.9% of Cl.

Table 2
Elemental concentration percent calculated by XPS.

Sample	Si	O	Cl
O1	50.7	45.4	3.9
O2	61.1	37.2	1.7
O3	45.3	49.5	5.2

*Uncertain estimated is 5% in standard deviation.

Due to specific conditions of preparation and growth of the samples, two oxidation states are not yet defined for the core level of Cl-$2p_2p_{3/2}$ with binding energies of 199.29 eV for samples O1 and O2 and a BE = 200.15 eV for sample O3, respectively. However, at the same time, no changes are observed in the binding energy of the silicon oxidation states (Fig.1), suggesting that the chlorine atoms form stable terminal bonds in *Si*-O-Cl promoting the oxidation and crystallinity of the film [25].

It is very probable that the terminal bonds of the chlorine in SiOx-Cl will be located at the grain boundary or at the boundary of the nanocrystal facing towards the amorphous zone of the polymorphous film. It could be the reason that in XPS two distinct oxidation states are observed for Cl-2p. The latter can also be seen in the form of superficial passivation of the grain boundaries and reason for the greater stability of the films with higher oxygen content.

3.2. SEM micrographs

The Fig. 2 shows cross section SEM images where comparison of the porosity in between the samples depending on the high (O_x) and low (N_x) oxygen concentration could be seen.

From Fig.2 differences in porosity for two samples with different oxygen concentrations (N2 and O1) grown at different hydrogen dilution (R_H of 93.8 and 95.2, respectively) and grown at same deposition pressure can be observed. Greater porosity can be observed for the sample O1. This visually confirms the fact that the films grown at high $R_{H,}$ which showed greater oxygen incorporation, tend to have a porous structure (as discussed earlier). Moreover, Table 1 shows that the high pressure and high hydrogen dilutions increase the growth rate and

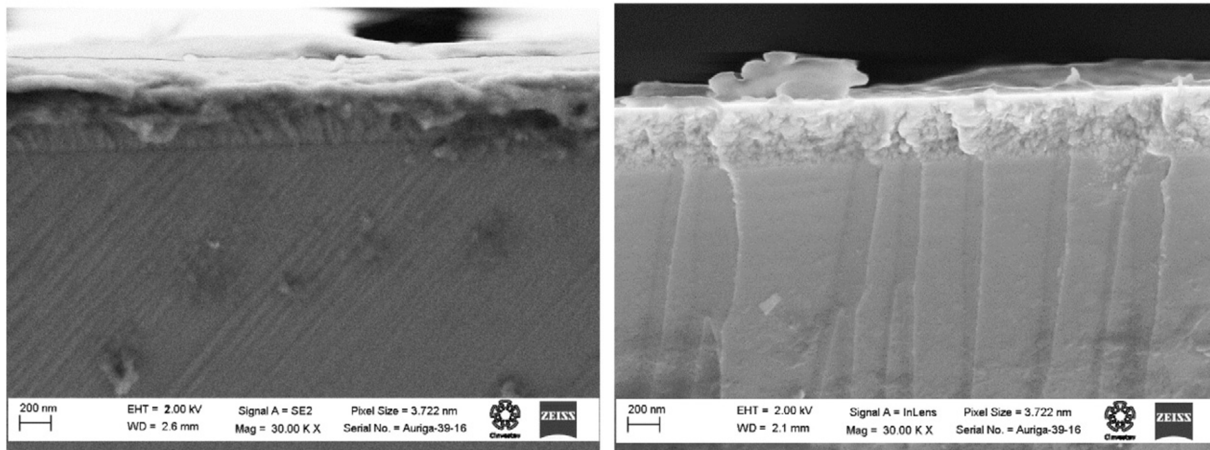

Fig. 2. Representative cross section SEM micrographs of porous oxidized films grown at (a) R_H of 93.8 (sample N2) and (b) R_H of 95.2 (sample O1).

enhance the formation of sub stoichiometric oxides (SiO_x) due to ambient exposure, which evidences occurrence of a higher porosity of the film. Here, the chlorine-terminated surface with a strong electronegative state reacts with residual oxygen and water vapor, which afterward forms SiO and SiH_xO_y complexes which could result in a disorder in the a-Si network. This signifies that most of the chlorine atoms were consumed for the formation of complex structures, as has been confirmed by the XPS analysis. The appearance of Si—O related peak in XPS is the outcome of porous structure formation, which facilitates the absorption of oxygen on the surface of microvoids when the films are exposed to the ambiance.

3.3. Fourier transform infrared spectroscopy, FTIR

Fig. 3 show the FTIR spectra of deposited samples accommodated in the increasing order of R_H for the two different pressures.

Fig. 3 exhibits the absence of Si—H stretching mode around 1900–2100 cm^{-1} for all of the deposited samples. This indicates a better stability in our samples because this band is related to weak hydrogen bonds that are prone to generate light induced degradation of the amorphous material [26]. Also, the Si_mH_n wagging mode around 620–640 cm^{-1} is present in all cases, along with the minute presence of the absorbance band related to $(Si—H_2)_n$ bending modes. All these modes have been correlated mainly with surface passivation of silicon nanocrystals in pm-Si:H thin films [10,27–29]. Of these measurements, it is visible that samples grown at lower hydrogen dilution (R_H) contain more hydrogen in the matrix and as-well on the surface of the nanocrystals. Here, the Si—Si bond breaking by atomic hydrogen enhances the chemical reactivity of SiCld (d: dangling bond) and/or SiHCl-related complexes more than that of SiHd, because of strong electron negativity of a chlorine atom. Apart from acting as a terminal bond, atomic Cl could correspondingly facilitate the removal of H atoms by breaking Si—H and Si—Si weak bonds which could cause photo-induced degradation of the material while promoting the formation of nanocrystalline phase.

On the other hand, in concordance with the XPS results, it can be observed in Fig. 4 that the samples O1, O2, and O3 have an absorption band between 1070 and 1200 cm^{-1} that is not evident for the films deposited at lower R_H. This band corresponds to Si–O–Si bond stretching vibration with a shoulder on the right-hand side due to the contribution of the LO Si—O vibration mode between 1107 and 1130 cm^{-1}. These particular absorption peaks have been termed as asymmetric stretching modes of the *Si*-O-Si bond [30–32].

Two Gaussian peaks were used (Fig. 4) for the deconvolution of this band to find the position of Si–O–Si stretching vibration and the asymmetric stretching modes of the Si-O-Si bond. This band corresponds to stretching Si—O absorption band, evidenced by a considerable amount of oxidation and can attribute to a more porous structure. Likewise, it supports the fact that the use of $SiCl_2H_2$ in the PECVD process favors the formation of nanoclusters within the growing film [23,32,33].

3.4. Optical band gap

The optical bandgap, E_g^{op}, of the films was calculated from absorbance measurements by the method of Tauc's plot, where E_g^{op} of each sample was estimated using the plot of $(\alpha h\nu)^{1/2}$ vs. $h\nu$ [20,21,34]. The

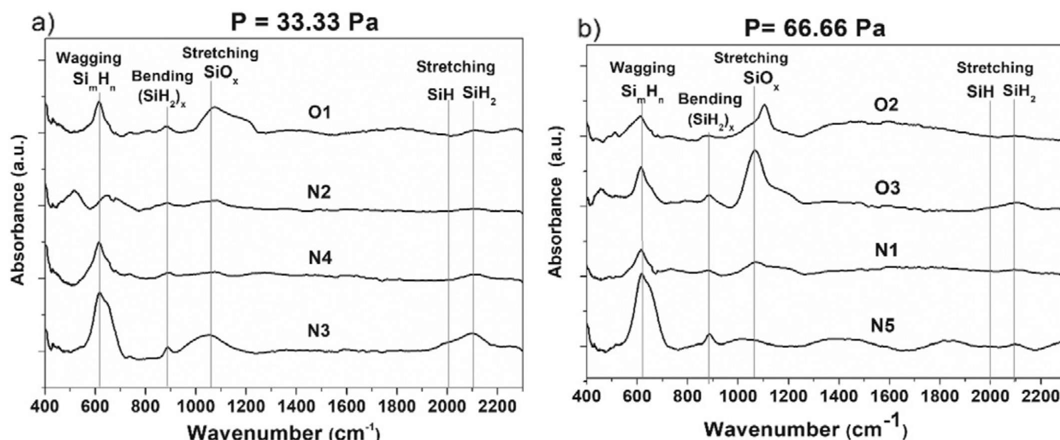

Fig. 3. Infrared spectra of pm-Si:H films deposited at a pressure of (a) 33.33 Pa and (b) 66.66 Pa showing the absorbance peaks for all samples.

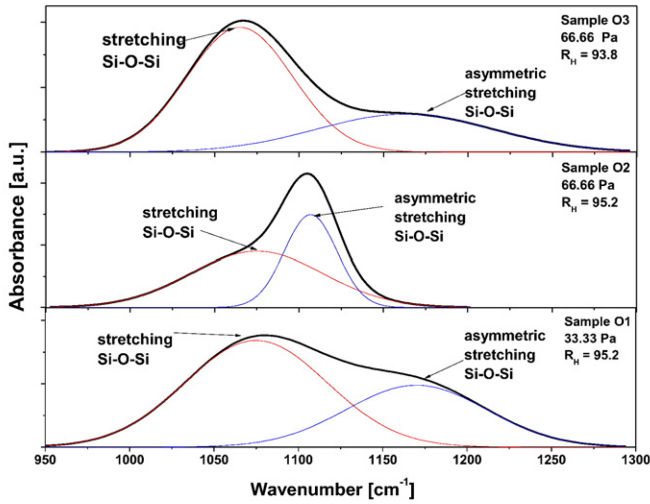

Fig. 4. Deconvolution of the FTIR characteristic peak at 1075 cm^{-1}. The FTIR spectra for samples O1, O2, and O3 were obtained from the FTIR spectrum of Fig. 2.

changes in E_g^{op} of the films prepared at various R_H values are presented in Fig. 5 as a function of the crystalline fraction, X_C, and the average size of nano-clusters, D_R

In Fig. 5 we can see how E_g^{op} is modified from 1.1–2.1 eV for the samples with low oxygen concentration (N1 to N5) achieving the highest optical band gap values. While, the samples O1, O2, and O3, attain E_g^{op} below of 1.6 eV, with the elevated structural parameters (X_C and D_R). In general, the optical band gap of pm-Si: H thin films could present a high range of variation because the material contains both amorphous and crystalline phases and their optical properties could vary corresponding to the structure of each of these phases. Accordingly, in the case of a mixed phase of crystalline and amorphous, i.e. nanocrystalline phase, the band gap should lie in between amorphous and crystalline silicon. The energy band gap,E_g, of c-Si is 1.12 eV, and the optical bandgap located between 1.5 and 2.0 eV is associated with the amorphous silicon matrix. Furthermore, changes in E_g^{op} depend on the form and content of hydrogen bonding. In the earlier experimental studies, the researchers have determined that the band gap can be additionally correlated to the total di-hydride content (Si—H_2) than local Si—Si bonding environments and the Si—H bonding [20,35]. However, our FTIR results did not show peaks related with di-hydride content. It suggests that in our case the variations observed in E_g^{op} are largely related to the presence of nanocrystalline phase in the thin films. To support this hypothesis, we can see in Fig. 5 how variations in E_g^{op} have a tendency to decrease with the increase in D_R of embedded nanoclusters which are randomly distributed in the amorphous network of pm-Si:H thin films. This behavior could be related to quantum confinement effect (Q.C.E). According to quantum confinement theory, the optical bandgap E_g^{op} depends on the size of the nc-Si as $E_g^{op} \approx E_g + \frac{\hbar^2\pi^2}{2\mu {D_R}^2}$; where E_g is the bulk material gap and μ is the reduced mass of electron-hole pair [20,32].

On the another hand, the observed E_g^{op}values in our oxygenated samples are slightly lower than the normally observed (1.7–1.8 eV) for films deposited by PECVD technique [36]. Herein, we show that Cl can be incorporated into pm-si:H, without provoking a significant change in its optical band gap, which is carried through abstraction and replacement of H by Cl species (generated by electron impact dissociation of SiH_2Cl_2 gas). There are two reasons for the change in the optical band gap in case of pm-Si:H(Cl) thin films as compared to pm-Si:H. One possibility is that the optical band gap is changed by the binding energy difference between bonding species, such as Si—Cl (4 eV), Si—H (3.4 eV) and Si—Si (2.2–2.4 eV). Another possibility could be due to differences in the Cl bonding configurations in films deposited from cholorosilanes; these different Cl bonding configurations may have an effect on the optical band gap [9,36].

Control of depositing thin films with a tunable band gap (varying the size distribution and the density of the nanocrystals) which can be

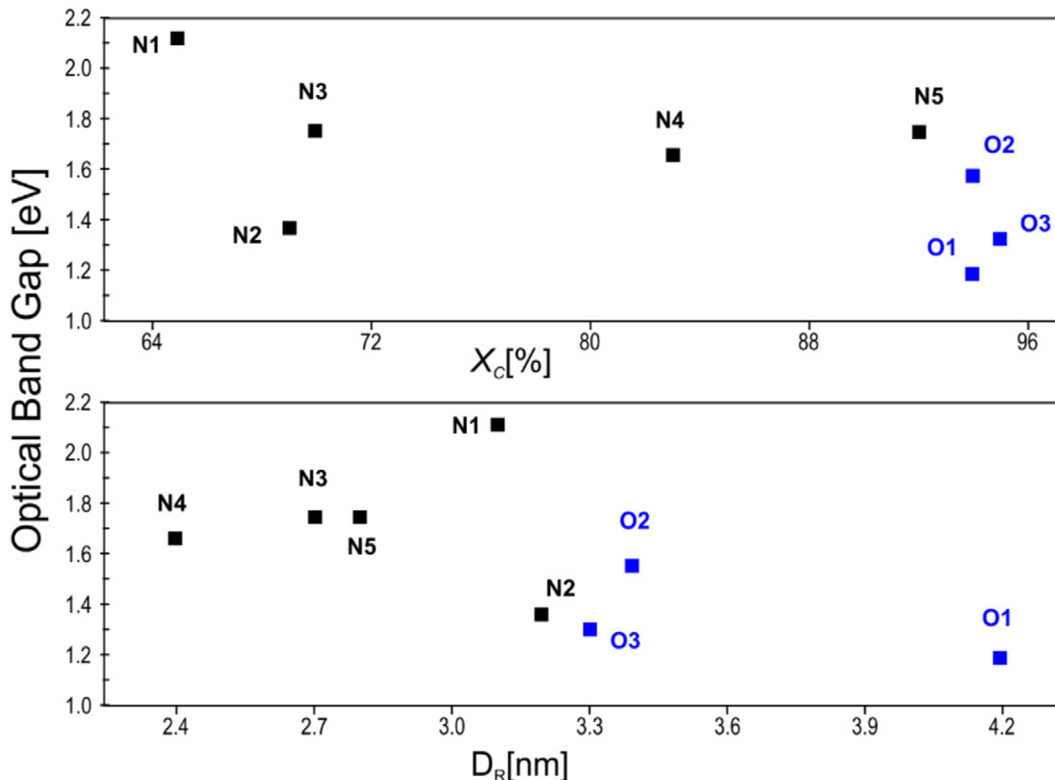

Fig. 5. Changes in the optical band gap, E_g^{op}as a function of X_C and D_R.

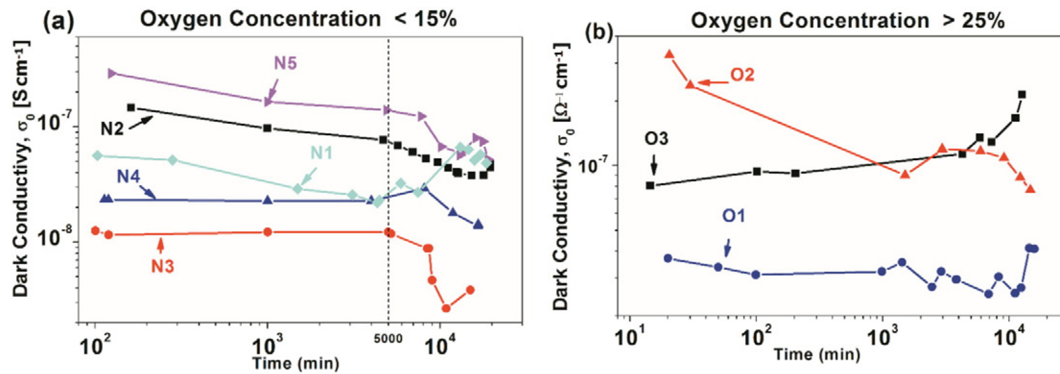

Fig. 6. Time-dependence of dark conductivity, σ_d, for pm-Si:H thin films separated by level of oxidation by hydrolysis reactions with ambient exposure in a) <15% and in b) above of 25%.

easily tailored by controlling the deposition parameters is useful for fabrication of tandem solar cells. Indeed the optical properties depend mainly on the amorphous matrix while the transport properties, such as the conductivity, are related to the crystallites size and density [37].

3.5. Dark conductivity

In order to study the impact of the level of oxidation by ambient exposure on dark conductivity (σ_d) further experiments have been carried out. Fig. 6 shows time-dependence σ_d for the samples with a) low and b) high oxygen concentrations.

Fig. 6 shows difference in the behaviors of σ_d for two ranges of oxygen concentration. For the samples N1 to N5 in Fig. 6 a), we can observe that σ_d remains stable for the first 5000 min, later it falls, except for sample N1, which is the only sample that has shown increment compared to other thin films. On the other hand, for the samples O1 and O3 in Fig. 6 b) we can see in general an increase in dark conductivity level (high oxygen concentration) compared to samples N1 to N5, besides, it also shows an improved stability in σ_d during all the time of measurement. However, under dark conductivity especially for the sample O2, tendency observed could be correlated with the lower oxygen concentration obtained from the Table 2 and from the Fig. 4.

The conductivity for the samples with high oxygen concentration can be stabilized and increased due to the contribution of three factors. i) Charge transport in highly conductive regions of crystalline material for samples which have shown the highest X_c in Table 1. ii) Conductivity is enhanced by tunneling in the barriers created by the amorphous material in between adjacent crystallite clusters. The electrons will tunnel between conductive regions at locations of closest approach. As well these samples have also shown the highest D_R (Table 1). iii) Conductivity is also promoted by the depletion regions formed between the interfaces of amorphous and crystalline regions, due to the electronegativity of oxygen which is incorporated as terminal bond.

3.6. Photoconductivity

Results of the photoconductivity, σ_{ph}, measurements as a function of illumination time using white light illumination of 100 mW/cm^2 (AM 1.5 condition) during continuous light 250 h are shown in Fig. 7. Fig. 7a) corresponds to the sample with a level of oxygen concentrations <15%, and in b) with a level of oxygen concentrations above than 25%. The temperature was controlled at 25 °C by heat dissipation.

Fig. 7 a) shows the photoconductivity response during firsts 5000 min for low oxygen concentration samples, whereas, for the longer duration drastic changes appear later to some of the samples. While in Fig. 7 b), for the samples O1 to O3, we observe σ_d remain stable with a gradual increase during all light soaking time due to the further oxidation of the samples.

These results show the contribution on the structural and optoelectronic properties of pm-Si:H thin films of different phases (amorphous, nanocrystalline), as well as of the passivation of these particular phases by oxygen. While for nanoparticles with bigger in dimensions, the surface area for interaction decreases, in the present case it appears that the contact and tunneling effect results in the conduction to increase overall. In addition, oxygen results in good surface passivation without leaving any dangling bonds behind. As mentioned above in Section 1, the decrease in a number of dangling bonds could increase the factor $\mu\tau$, which could subsequently affect the diffusion length of minority carriers in the device. From Fig. 7 (b), the effect of oxygen passivation on the positive increase of the photoconductivity confirms the above theory.

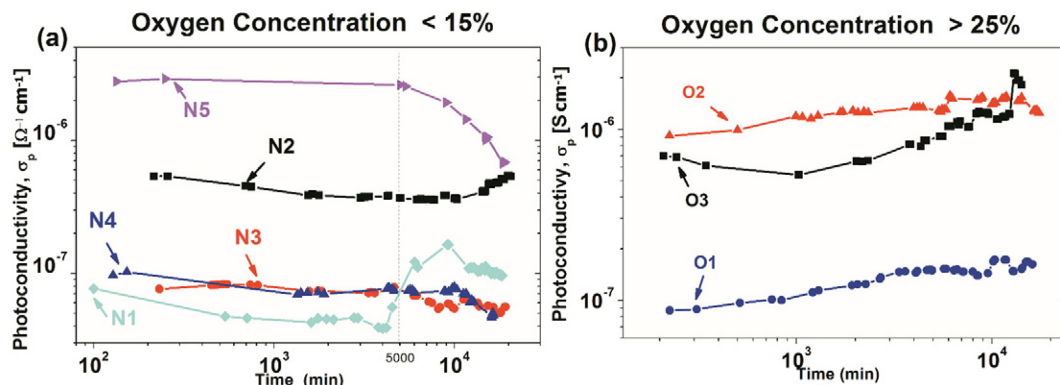

Fig. 7. Photoconductivity versus illumination time for pm-Si: H thin films separated by level of oxidation obtained by hydrolysis reactions with ambient exposure. In a) <15% and in b) >25%.

4. Conclusion

In summary, the influence of oxygen incorporation on the structural, optical and electrical properties of pm-Si: H layer deposited by PECVD is investigated. Using FTIR and XPS analysis, chemical composition and oxidation state (Si, O, and Cl) of the polymorphous thin films has been determined, respectively. From FTIR analysis, absence of weak silicon hydride (Si—H) bonds while the presence of absorption bond related to Si_mH_n was clearly observed. This result is largely related to the better stability of our samples. As well, it was found that the residual chlorine atoms induce a higher degree of disorder of a-Si:H:Cl network and promotes the SiO and SiOH complex formation. Samples were subdivided into two different groups depending on the oxygen concentration. Finally, conductivity measurements carried out on the pm-Si:H thin films revealed that the samples with higher oxygen concentration shown increment in conductivity and photostability as an effect of the light soaking experiment. Study realized in the present work provides the basis of detailed chemical study and stability of pm-Si:H thin films (with oxygen presence) for their use as in the practical implementation of silicon solar cells in the modern world.

Acknowledgments

We acknowledge partial financial support for this work from DGAPA-UNAM PAPIIT Projects IN108215 and IN107017. We would express our sincere thanks to Josué E. Romero-Ibarra for SEM measurements and C. D. Ramos Vilchis for technical assistance. A special acknowledgment is due to financial support from CONACyT through doctoral scholarship CVU 517361 and 445952, and thesis fellowships. A. Dutt acknowledges to DGAPA postdoctoral scholarship and assistance.

References

[1] W. Bronner, J. Kleider, R. Brüggemann, P. Roca i Cabarrocas, D. Mencaraglia, and M. Mehring, Comparison of transport and defects properties in hydrogenated polymorphous and amorphous silicon, J. Non-Cryst. Solids 299–302 (2002) 551–555.
[2] K. Morigaki, K. Takeda, H. Hikita, P. Roca, Light-induced defect creation in hydrogenated polymorphous silicon, Mater. Sci. Eng. B 121 (2005) 34–41.
[3] B.M. Monroy, G. Santana, J. Fandiño, A. Ortiz, J.C. Alonso, Growth of silicon nanoclusters on different substrates by plasma enhanced chemical vapor deposition, J. Nanosci. Nanotechnol. 6 (2006) 4–7.
[4] E.V.Ã. Johnson, L. Kroely, P.R. Cabarrocas, Solar energy materials & solar cells Raman scattering analysis of SiH bond stretching modes in hydrogenated microcrystalline silicon for use in thin-film photovoltaics, Sol. Energy Mater. Sol. Cells 93 (2009) 1904–1906.
[5] J. Kumar Saha, N. Ohse, K. Hamada, H. Matsui, T. Kobayashi, H. Jia, H. Shirai, Fast deposition of microcrystalline Si films from SiH2Cl2 using a high-density microwave plasma source for Si thin-film solar cells, Sol. Energy Mater. Sol. Cells 94 (2010) 524–530.
[6] L. Zhang, J.H. Gao, J.Q. Xiao, L.S. Wen, J. Gong, C. Sun, Low-temperature (120 °C) growth of nanocrystalline silicon films prepared by plasma enhanced chemical vapor deposition from SiCl4/H2 gases: microstructure characterization, Appl. Surf. Sci. 258 (2012) 3221–3226.
[7] C. Álvarez-Macias, J. Santoyo-Salazar, B. Monroy, M. Garcia-Sánchez, M. Picquart, A. Ponce, G. Contreras-Puente, G. Santana, Estructura y morfología de películas de pm-Si: H crecidas por PECVD variando la dilución de diclorosilano con hidrógeno y la presión de trabajo, Rev. Mex. Fis. 57 (2011) 224–231.
[8] T. Ito, K. Hashimoto, H. Shirai, Surface chemistry of Si:H:Cl film formation by RF plasma-enhanced chemical vapor deposition of SiH 2 cl 2 and SiCl 4, Jpn. J. Appl. Phys. 42 (2003) L1119–L1122.
[9] A. Takano, T. Wada, S. Fujikake, T. Yoshida, T. Ohto, E.S. Aydil, Reaction Control in Amorphous Silicon Film Deposition by Hydrogen Chloride, MRS Proceedings 762, 2003.
[10] C. Álvarez-Macias, B.M. Monroy, L. Huertaa, M. Canseco-Martínez, M. Picquart, J. Santoyo-Salazar, M.F. García Sánchez, G. Santana, Chemical and structural properties of polymorphous silicon thin films grown from dichlorosilane, Appl. Surf. Sci. 285-B (2013) 431–439.
[11] A. Fontcuberta i Morral, H. Hofmeister, P. Roca i Cabarrocas, Structure of plasma-deposited polymorphous silicon, J Non.Cryst. Solids 299–302 (2002) 284–289.
[12] G. Viera, S. Huet, L. Boufendi, Crystal size and temperature measurements in nanostructured silicon using Raman spectroscopy J, Appl. Phys. 90 (2001) 4175.
[13] E. Mon-Perez, J. Salazar, E. Ramos, J. Santoyo Salazar, A. López Suárez, A. Dutt, G. Santana, B. Marel Monroy, Nanotechnology 27 (2016) 455703.
[14] H. Shirai, Role of chlorine in the nanocrystalline silicon film formation by rf plasma-enhanced chemical vapor deposition of chlorinated materials, Thin Solid Films 457 (2004) 90–96.
[15] J. Fang, Z. Chen, N. Wang, L. Bai, G. Hou, X. Chen, C. Wei, G. Wang, J. Sun, Y. Zhao, X. Zhang, Improvement in performance of hydrogenated amorphous silicon solar cells with hydrogenated intrinsic amorphous silicon oxide p/i buffer layers, Sol. Energy Mater. Sol. Cells 128 (2014) 394–398.
[16] Y.-H. Chen, Y.-T. Liu, C.-F. Huang, J.-C. Liu, C.-C. Lin, Improved photovoltaic properties of amorphous silicon thin-film solar cells with an un-doped silicon oxide layer, Mater. Sci. Semicond. Process. 31 (2015) 184–188.
[17] J.E. Lee, J.H. Park, J. Yoo, K.H. Yoon, D. Kim, J.-S. Cho, The deposition of intrinsic hydrogenated amorphous silicon thin films incorporated with oxygen by plasma-enhanced vapor deposition, Solid State Sci. 20 (2013) 70–74.
[18] J. Woerdenweber, T. Merdzhanova, A. Gordijn, H. Stiebig, W. Beyer, Incorporation and critical concentration of oxygen in a-Si:H solar cells, Sol. Energy Mater. Sol. Cells 95 (2011) 2811–2815.
[19] B. Pivac, I. Kovacevic, I. Zulim, Defects induced in amorphous silicon thin films by light soaking, Thin Solid Films 403–404 (2002) 513–516.
[20] A. Remolina, B.M. Monroy, M.F. García-Sánchez, A. Ponce, M. Bizarro, J.C. Alonso, A. Ortiz, G. Santana, Polymorphous silicon thin films obtained by plasma-enhanced chemical vapor deposition using dichlorosilane as silicon precursor, Nanotechnology 20 (2009) 245604.
[21] B. Yan, L. Zhao, B. Zhao, J. Chen, G. Wang, H. Diao, Y. Mao, W. Wang, Hydrogenated amorphous silicon germanium alloy with enhanced photosensitivity prepared by plasma enhanced chemical vapor deposition at high temperature, Vacuum 89 (2013) 43–46.
[22] F. Gao, V. Andrew, Teplyakov dehydrohalogenation condensation reaction of phenylhydrazine with Cl-terminated Si(111) surfaces, J. Phys. Chem. C 120 (2016) 5539–5548.
[23] W. Peng, S.M. Rupich, N. Shafiq, Y.N. Gartstein, A.V. Malko, Y.J. Chabal, Silicon surface modification and characterization for emergent photovoltaic applications based on energy transfer, Chem. Rev. 115 (2015) 12764–12796.
[24] M.P. Seah, Quantitative AES and XPS: convergence between theory and experimental databases, J. Electron Spectrosc. 100 (1999) 55–73.
[25] S.R. Amy, D.J. Michalak, Y.J. Chabal, Investigation of the reactions during alkylation of chlorine-terminated silicon (111) surfaces, J. Phys. Chem. C 111 (2007) 13053–13061.
[26] V.S. Waman, M.M. Kamble, M.R. Pramod, S.P. Gore, A.M. Funde, R.R. Hawaldar, D.P. Amalnerkar, V.G. Sathe, S.W. Gosavi, S.R. Jadkar, Influence of the deposition parameters on the microstructure and opto-electrical properties of hydrogenated nanocrystalline silicon films by HW-CVD, J. Non-Cryst. Solids 21 (2011) 3616–3622.
[27] B.W. Clare, J.C.L. Cornish, G.T. Hefter, P.J. Jennings, C.P. Lund, D.J. Santjojo, M.O.G. Talukder, Studies of photodegradation in hydrogenated amorphous silicon, Thin Solid Films 288 (1996) 76–82.
[28] J.H. Shim, S. Im, N.H. Cho, Nanostructural features of nc-Si: H thin films prepared by PECVD, Appl. Surf. Sci. 234 (2004) 268–273.
[29] A. Ali, Mechanisms of the growth of nanocrystalline Si:H films deposited by PECVD, J. Non-Cryst. Solids 352 (2006) 3126–3133.
[30] M. Modreanu, M. Gartner, E. Aperathitis, N. Tomozeiu, M. Androulidaki, Investigation on preparation and physical properties of nanocrystalline Si═SiO 2 superlattices for Si-based light-emitting devices, Physica E Low Dimens Syst Nanostruct. 16 (2003) 461–466.
[31] G. Mattei, V. Valentini, V.A. Yakovlev, An FTIR study of porous silicon layers exposed to humid air with and without pyridine vapors at room temperature, Surf. Sci. 502–503 (2002) 58–62.
[32] K. Kulathuraan, K. Mohanraj, B. Natarajan, Structural, optical and electrical characterization of nanostructured porous silicon: effect of current density, Spectrochim. Acta A Mol. Biomol. Spectrosc. 152 (2016) 51–57.
[33] V. Kapaklis, Structural characterization of silicon nanocrystals from amorphous silicon oxide materials, J. Non-Cryst. Solids 354 (2008) 612–617.
[34] Z.X.Ã. Zhao, R.Q. Cui, F.Y. Meng, Z.B. Zhou, H.C. Yu, T.T. Sun, Nanocrystalline silicon thin films deposited by high-frequency sputtering at low temperature, Sol. Energy Mater. 86 (2005) 135–144.
[35] K. Fukutani, M. Kanbe, W. Futako, B. Kaplan, T. Kamiya, C.M. Fortmann, I. Shimizu, Band gap tuning of a-Si:H from 1.55 eV to 2.10 eV by intentionally promoting structural relaxation, J. Non-Cryst. Solids 227–230 (1998) 63–67.
[36] A. Takano, T. Wada, S. Fujikake, T. Yoshida, T. Ohto, S. Barbara, Chlorine containing hydrogenated amorphous silicon without optical band gap widening, 3rd World Conference on Photovoltaic Energy Conversion Proceedings of Osaka, Japan 2003, pp. 1619–1622.
[37] L. Hamui, A. Remolina, M.F. García-Sánchez, A. Ponce, M. Picquart, M. López-López, B.M. Monroy, G. Santana, Deposition, opto-electronic and structural characterization of polymorphous silicon thin films to be applied in a solar cell structure, Mater. Sci. Semicond. Process. 30 (2015) 85–91.